The Astrophysical Journal Letters, 893:L26 (7pp), 2020 April 10 https://doi.org/10.3847/2041-8213/ab83fb

A Binary Comb Model for Periodic Fast Radio Bursts

Kunihito Ioka[1] and Bing Zhang[1,2]
[1] Center for Gravitational Physics, Yukawa Institute for Theoretical Physics, Kyoto University, Kyoto 606-8502, Japan; kunihito.ioka@yukawa.kyoto-u.ac.jp
[2] Department of Physics and Astronomy, University of Nevada Las Vegas, Las Vegas, NV 89154, USA
Received 2020 February 24; revised 2020 March 22; accepted 2020 March 27; published 2020 April 14

Abstract

We show that the periodic FRB 180916.J0158+65 can be interpreted by invoking an interacting neutron star binary system with an orbital period of ∼16 days. The FRBs are produced by a highly magnetized pulsar, whose magnetic field is "combed" by the strong wind from a companion star, either a massive star or a millisecond pulsar. The FRB pulsar wind retains a clear funnel in the companion's wind that is otherwise opaque to induced Compton or Raman scatterings for repeating FRB emission. The 4 day active window corresponds to the time when the funnel points toward Earth. The interaction also perturbs the magnetosphere of the FRB pulsar and may trigger emission of FRBs. We derive the physical constraints on the comb and the FRB pulsar from the observations and estimate the event rate of FRBs. In this scenario, a lower limit on the period of observable FRBs is predicted. We speculate that both the intrinsic factors (strong magnetic field and young age) and the extrinsic factor (interaction) may be needed to generate FRBs in neutron star binary systems.

Unified Astronomy Thesaurus concepts: Radio transient sources (2008); Binary pulsars (153); Neutron stars (1108); Magnetars (992); Non-thermal radiation sources (1119); Relativistic mechanics (1391); Magnetic fields (994); Periodic orbit (1212)

1. Introduction

Fast radio bursts (FRBs) are cosmological radio transients whose origin is enigmatic (Lorimer et al. 2007; Thornton et al. 2013; Cordes & Chatterjee 2019; Petroff et al. 2019). Regardless of their origin, these bursts can be useful probes for studying cosmology (Ioka 2003; Inoue 2004).

The recent discovery of the periodic repeating FRB 180916.J0158+65 (The CHIME/FRB Collaboration et al. 2020) may bring clues for understanding the source and emission mechanism of repeating FRBs. This source is harbored in a star-forming region of a nearby massive spiral galaxy at $z = 0.0337 \pm 0.0002$, with a luminosity distance of 149.0 ± 0.9 Mpc and a projected size of ∼1.5 kpc (Marcote et al. 2020). Twenty-eight bursts were detected from 2018 September 16 to 2019 October 30 by CHIME, which show a period of

$$P = 16.35 \pm 0.18 \text{ days}, \quad (1)$$

with a ∼4 day active time window. The average observed burst rate is[3] $\dot{N} \sim 25\ \mathrm{yr}^{-1}$.

In the literature, magnetars are usually invoked to interpret repeating FRB sources (e.g., Popov & Postnov 2013; Katz 2016; Murase et al. 2016; Kashiyama & Murase 2017; Kumar et al. 2017; Metzger et al. 2017). Alternatively, interaction between an astrophysical stream and neutron star magnetic field (the so-called "cosmic comb")[4] has been invoked to interpret repeating FRBs (Zhang 2017, 2018).

Here we propose a binary comb model for the periodic FRB 180916.J0158+65. We interpret the observed period in Equation (1) as the orbital period of a binary system that includes a neutron star for repeating FRBs (the FRB pulsar)[5] and a companion whose strong wind imposes a comb on the FRB pulsar. The interaction causes both modulation of FRB emission beams and probably also the triggers of FRB emission. We consider the cases that the companion star is either a massive star or a millisecond pulsar. A similar scenario was discussed by Lyutikov et al. (2020). Alternatively, the ∼16 day period was interpreted as the period of a magnetar due to either free precession (Levin et al. 2020; Zanazzi & Lai 2020) or orbital precession (Yang & Zou 2020). Another model attributes the periodicity to the precession of the jet launched from the accretion disk of a massive black hole (Katz 2020).

2. Physical Properties of the Binary Comb

2.1. Binary Separation

With the observed period (Equation (1)) identified as the binary orbital period, the semimajor axis of the binary is

$$a = (GM)^{1/3}(P_{\rm orb}/2\pi)^{2/3} \sim 4 \times 10^{12}\ \mathrm{cm}\ M_{\rm l}^{1/3} P_{\rm orb,16}^{2/3}, \quad (2)$$

where $M = m_A + m_B = 10 M_\odot M_{\rm l}$ is the total mass of the binary and $P_{\rm orb,16} = P_{\rm orb}/16$ days. The separation between the stars ranges from $a_{\rm min} = a(1-e)$ to $a_{\rm max} = a(1+e)$ for an eccentricity e. For a massive star companion, the total mass is $M \sim$ (10–50) $M_\odot$. For main-sequence stars, the stellar radius is about $\sim 3 \times 10^{11}\ \mathrm{cm}\ M_{\rm l}^{0.57}$ for $M_1 \gtrsim 0.1$ (Kippenhahn & Weigert 1990), which is smaller than the binary separation. For a neutron star companion, the total mass is $M \sim 2.8 M_\odot$ and hence $a \sim 2.6 \times 10^{12}$ cm.

[3] The true rate would be at least an order of magnitude greater than $\sim 25\ \mathrm{yr}^{-1}$ because CHIME observes the source location a few hours per day and because there could be fainter bursts below the CHIME flux sensitivity.
[4] In addition to "interaction," we also use "comb" because it gives the visual impression of the interaction (see Figure 1).
[5] We use "FRB pulsar" because the FRB-emitting sources in our model include both young, high-magnetic-field pulsars and magnetars.

2.2. Optical Depth

2.2.1. Massive Star Companion

For a massive star case, the wind density around the FRB source is

$$n_w(0) \sim \frac{\dot{M}}{4\pi a^2 m_p V} \sim 9 \times 10^5\,\mathrm{cm^{-3}}\,\dot{M}_{-9} a_{12.6}^{-2} V_{3.3}^{-1}, \quad (3)$$

where $a_{12.6} = a/4 \times 10^{12}$ cm, $V = 2 \times 10^3\,\mathrm{km\,s^{-1}}\,V_{3.3}$ is the wind velocity, and m_p is the proton mass. We adopt a mass-loss rate $\dot{M} = 10^{-9} M_\odot\ \mathrm{yr^{-1}} M_{-9}$ of main-sequence B stars as the fiducial value because they are popular (see also Section 4.1). Note that the mass-loss rate of O7 and later stars is a factor of 10–10^2 lower than theoretically expected (Puls et al. 2008; Smith 2014). The B star becomes a rapidly rotating Be star through a mass-exchange episode before the FRB pulsar is born (e.g., Postnov & Yungelson 2014). The equatorial mass-loss rates of Be stars may be larger by a factor of $\sim 10^2$ (Nieuwenhuijzen & de Jager 1988).

The optical depth to Thomson scattering is small $\tau_\mathrm{T} \sim \sigma_\mathrm{T} n_w(0)\, a \sim 2 \times 10^{-6}$ around the FRB source where σ_T is the Thomson cross section. The optical depth to free–free absorption is $\tau_\mathrm{ff} \sim a\alpha_\nu^\mathrm{ff} \sim 0.06\,\bar{g}_\mathrm{ff} T_4^{-3/2} \nu_9^{-2}$ for fiducial parameters where $\alpha_\nu^\mathrm{ff} = (4q^6/3m_e kc)(2\pi/3km_e)^{1/2} T^{-3/2} n_w(0)^2 \nu^{-2} \bar{g}_\mathrm{ff}$ is the free–free absorption coefficient at frequency $\nu = 1$ GHz ν_9 and temperature $T = 10^4$ K T_4 (Lyutikov et al. 2020).

More important are the induced scattering processes (Wilson & Rees 1978; Thompson et al. 1994; Lyubarsky 2008) because the brightness temperature of the FRB is extremely high (e.g., $T_\mathrm{FRB} \sim 10^{32}$ K) and the scattering probability of bosons is enhanced by the occupation number of the final state $kT_\mathrm{FRB}/h\nu \sim 2 \times 10^{33}\, T_\mathrm{FRB,32} \nu_9^{-1}$. The optical depth to the induced Compton scattering at a radius $r = 10^{13}\,\mathrm{cm}\, r_{13}$ is estimated by

$$\tau_C \sim \frac{3\sigma_T}{32\pi^2} \frac{n_w(r) L c \Delta t}{r^2 m_e \nu^3} \sim 30\, \dot{M}_{-9} V_{3.3}^{-1} r_{13}^{-4} (L\Delta t)_{38} \nu_9^{-3}, \quad (4)$$

where $L\Delta t = 10^{38}\,\mathrm{erg}(L\Delta t)_{38}$ is the FRB isotropic luminosity times duration, and the wind density decreases as $n_w(r) \sim n_w(0)[a/(a+r)]^2$ ($\propto r^{-2}$ at $r \gg a$). Here r is measured from the FRB source, not from the companion. Using a simple criterion for observability $\tau_C < 10$ (Lyubarsky 2008), the photospheric radius for the induced Compton scatterings is

$$r_\mathrm{ph}^C \sim 1 \times 10^{13}\,\mathrm{cm}\,(L\Delta t)_{38}^{1/4} \dot{M}_{-9}^{1/4} V_{3.3}^{-1/4} \nu_9^{-3/4}. \quad (5)$$

The above expression is easy to understand as follows. The photon occupation number is given by

$$\mathcal{N} = \frac{c^2 L_\nu}{8\pi^2 \theta_b^2 r^2 h \nu^3} \sim \frac{c^2 L}{8\pi^2 \theta_b^2 r^2 h \nu^4}, \quad (6)$$

where L_ν is the isotropic specific luminosity. For induced Compton scattering, the scattered photon lies within the half-opening angle of the photon beam θ_b, so that the cross section is $\sigma_C \sim \sigma_\mathrm{T} \mathcal{N} \theta_b^2/4$. In each scattering, a photon loses a fraction $\varepsilon_C \sim h\nu\theta_b^2/2m_e c^2$ of its energy. Then the effective optical depth is estimated by $\tau_C \sim \varepsilon_C \sigma_C n_w r$, which reproduces Equation (4) within a factor of $\pi/3$ if we replace $r\theta_b^2/2$ by $c\Delta t$ because the induced scattering occurs only if the scattered ray remains within the zone illuminated by the scattering radiation (Lyubarsky 2008). If $\theta_b < (2c\Delta t/r)^{1/2} \sim 8 \times 10^{-3} (\Delta t/10\ \mathrm{ms})^{1/2} r_{13}^{-1/2}$, this replacement is not necessary. Note that the Planck constant h is canceled in the product of $\mathcal{N}$ and ε_C.

The induced Raman scattering by emitting Langmuir waves could be even more significant. The optical depth at $r = 10^{14}$ cm r_{14} is estimated by

$$\tau_R \sim \tau_C \nu/\nu_p \sim 9\, \dot{M}_{-9}^{1/2} V_{3.3}^{-1/2} r_{14}^{-3} (L\Delta t)_{38} \nu_9^{-2}, \quad (7)$$

where $\nu_p = [q^2 n_w(r)/(\pi m_e)]^{1/2}$ is the plasma frequency, if the scattering angle is not too small and the decay of plasmons is weak (Thompson et al. 1994; Lyubarsky 2008). The photospheric radius for induced Raman scattering is

$$r_\mathrm{ph}^R \sim 1 \times 10^{14}\,\mathrm{cm}\,(L\Delta t)_{38}^{1/3} \dot{M}_{-9}^{1/6} V_{3.3}^{-1/6} \nu_9^{-2/3}. \quad (8)$$

Note that the Raman scattering effect just widens the beam to $\theta_b \sim 6 \times 10^{-2} (n_w(r)/10^3\,\mathrm{cm^{-3}})^{1/2} T_4^{-1/2}$ but temporally smears a pulse to $\sim r\theta_b^2/2c > \Delta t$.

The photosphere $r_\mathrm{ph} \sim 10^{13}$–$10^{14}$ cm is larger than the separation a in Equation (2) for fiducial parameters. It is also remarkable that the photosphere is larger than the separation even for a Sun-like star with $\dot{M} \sim 2 \times 10^{-14} M_\odot\ \mathrm{yr^{-1}}$, $M \sim 2.4 M_\odot$, and $V \sim 800$ km s^{-1}. Therefore, the stellar wind basically makes the system optically thick.

2.2.2. Neutron Star Companion

For the neutron star companion case, the wind density around the FRB source at $a \sim 2.6 \times 10^{12}\,\mathrm{cm}\, a_{12.4}$ is

$$n_w(0) \sim \frac{L_w}{4\pi a^2 m_e c^2 V \Gamma (1+\sigma)} \sim \frac{5 \times 10^3\,\mathrm{cm^{-3}}}{\Gamma(1+\sigma)} L_{w,34} a_{12.4}^{-2}, \quad (9)$$

where we take $V \sim c$, $\Gamma = [1 - (V/c)^2]^{-1/2}$ is the Lorentz factor of the wind, and σ is the ratio of Poynting flux to particle energy flux. For the fiducial value of the wind luminosity, we take that of a typical millisecond pulsar $L_w = 10^{34} L_{w,34}$, because a millisecond pulsar is usually formed in a neutron star binary system and is the one with the higher spin-down rate as observed in our Galaxy (e.g., Tauris et al. 2017).

The optical depth to the induced Compton scattering is easy to estimate in the comoving frame of the wind to take relativistic effects into account,

$$\tau_C \sim \frac{3\sigma_T}{32\pi^2} \frac{n_w'(r) L' c \Delta t'}{r'^2 m_e \nu'^3} \sim \frac{8\delta^2}{\Gamma^2(1+\sigma)} L_{w,34} r_{12.5}^{-4} (L\Delta t)_{38} \nu_9^{-3}, \quad (10)$$

where the relations with the lab-frame quantities are $L' = L/\delta^4$, $\nu' = \nu/\delta$, $\Delta t' = \delta \Delta t$, $r' = r/\delta$, and $n_w' = n_w/\Gamma$, and $\delta = [\Gamma(1 - (V/c)\cos\theta_w)]^{-1}$ is the Doppler factor for an angle θ_w between the photon and the wind direction. Note that L/r^2 transforms as a flux. The photosphere is located at

$$r_\mathrm{ph}^C \sim 2 \times 10^{12}\,\mathrm{cm}\,\delta^{1/2} \Gamma^{-1/2} (1+\sigma)^{-1/4} L_{w,34}^{1/4} (L\Delta t)_{38}^{1/4} \nu_9^{-3/4} \quad (11)$$

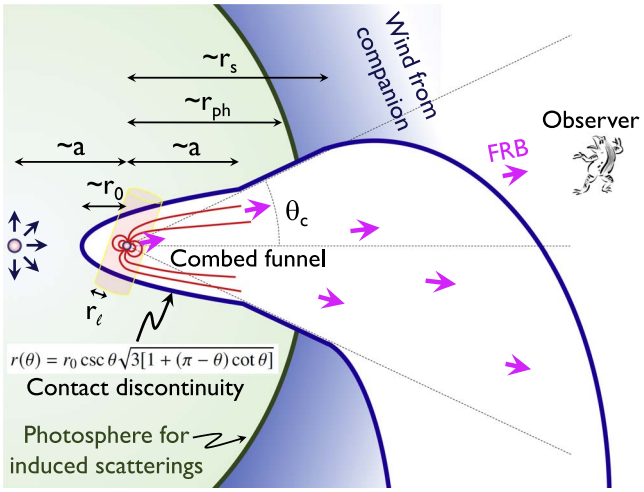

Figure 1. Binary comb model for the periodic FRB 180916.J0158+65. The wind from the FRB pulsar creates a clean funnel with a half-opening angle θ_c, which is combed by the wind from the companion. There are several characteristic scales: r_ℓ is the radius of the light cylinder, r_0 is the minimum comb size on the side of the companion, a is the separation to the companion and is also the radius of the comb opening, $r_{\rm ph}$ is the photospheric radius to induced scatterings, and r_s is the spiral radius due to orbital motion.

The photospheric radius for the induced Raman scattering is estimated from $\tau_R \sim \tau_C \nu'/\nu'_p \sim 10$ as

$$r_{\rm ph}^R \sim 3 \times 10^{13}\,{\rm cm}\,\delta^{1/3}\Gamma^{-1/3}(1+\sigma)^{-1/6}L_{w,34}^{1/6}(L\Delta t)_{38}^{1/3}\nu_9^{-2/3}. \quad (12)$$

Note that $\delta \sim \Gamma$ for $\theta_w \ll \Gamma^{-1}$, and $\delta \sim 2/(\Gamma\theta_w^2)$ for $\theta_w \gg \Gamma^{-1}$. Although the Lorentz factor Γ and magnetization parameter σ are quite uncertain, the dependence is weak, so that the pulsar wind makes the system optically thick and temporally smears a pulse to $\sim r_{\rm ph}\theta_w^2/2c > \Delta t$ for a large parameter space.

For the wind from the FRB pulsar, the Doppler factor is $\delta \sim \Gamma$ since $\theta_w \sim 0$. An FRB pulse is likely generated below the photosphere and is temporally smeared to $\sim r_{\rm ph}/2c\Gamma^2$ via scatterings. However, this is shorter than the pulse width Δt for large Lorentz factors, and the FRB pulsar itself is observable.

2.3. Comb Size Required by Duty Cycle

The wind from the companion basically makes the system optically thick. In order to make an FRB observable by an Earth observer, the wind from the FRB pulsar should open a way to the observer. Namely, a cosmic comb retains a clear funnel for the FRB to propagate (Figure 1). Since all the bursts arrive in a 4 day phase window of the 16 day period, the half-opening angle of the comb should be[6]

$$\theta_c \gtrsim \pi/4. \quad (13)$$

In principle, the opening angle can be arbitrarily small for a highly eccentric orbit because the polar angle swept by the FRB pulsar during the 4 day phase becomes smaller for higher eccentricity around the apocenter. In this case the observable viewing angle is also small.

Near the FRB pulsar with a distance much smaller than the binary separation, the comb structure is obtained by a problem that a wind-blowing star moves with a constant velocity in a uniform density. The shape of the contact discontinuity is obtained analytically as

$$r(\theta) = r_0 {\rm csc}\theta\sqrt{3[1+(\pi-\theta){\rm cot}\,\theta]}, \quad (14)$$

in a thin shock limit (Wilkin 1996), where $r(\theta)$ is the distance from the FRB pulsar, θ is the polar angle from the axis of symmetry, and r_0 is the minimum size at $\theta = \pi$ (toward the companion). This solution is consistent with numerical simulations of pulsar bow shocks (Bucciantini 2002; Vigelius et al. 2007).

The above solution is applicable only up to the binary separation $r(\theta) \sim a$ because the radial dependence of the companion's wind becomes similar to that of the wind from the FRB pulsar (i.e., the approximation of a uniform density breaks down). Because of the same radial dependence (e.g., fluxes $\propto r^{-2}$), the polar angle of the contact discontinuity asymptotically becomes constant, which determines the opening angle of the comb (Figure 1). Requiring $r(\pi/4) \gtrsim a$ based on Equation (13), we find that the comb size on the side of the companion should be larger than

$$r_0 \gtrsim 0.22a \sim 9 \times 10^{11}\,{\rm cm}\,M_1^{1/3}P_{\rm orb,16}^{2/3}. \quad (15)$$

We stress that the above condition is a necessary condition. The duty cycle is also related to the solid angle $\Delta\Omega$ in which the bulk of FRBs are concentrated. (Note that this is different from the beaming angle of each FRB $\delta\Omega \sim \pi\theta_b^2$.) This is even implied by the observations because the European Very-long-baseline-interferometry Network (EVN) at 1.7 GHz detected bursts at the leading edge of the activity cycle observed at 400–800 MHz, while the Effelsberg radio telescope at 1.4 GHz detected no bursts during the middle of the cycle (The CHIME/FRB Collaboration et al. 2020). Only a plasma eclipse cannot explain the high-frequency deficit in the middle phase because high-frequency photons are generally transmittable. However, we should await more observations to confirm the periodicity at high frequencies.

On the other hand, in order for the FRB pulsar to be combed, the companion wind pressure must win at half of the separation, so that the comb size should satisfy

$$r_0 \lesssim 0.5a \sim 2 \times 10^{12}\,{\rm cm}\,M_1^{1/3}P_{\rm orb,16}^{2/3}. \quad (16)$$

Therefore, if the comb triggers FRBs, the comb size is constrained to a relatively narrow range $0.22a \lesssim r_0 \lesssim 0.5a$ in Equations (15) and (16). Remember that the eccentricity relaxes the lower limit while the inclination tightens it.

One more necessary condition arises because the comb tail is spiraled by the orbital motion at a radius

$$r_s \sim \frac{VP_{\rm orb}}{2\pi}\frac{\theta_c}{\pi/4} \sim 4 \times 10^{13}\,{\rm cm}\,P_{\rm orb,16}V_{3.3}(4\theta_c/\pi), \quad (17)$$

for the massive star case, and $r_s \sim 7 \times 10^{15}$ cm $P_{\rm orb,16}(4\theta_c/\pi)$ for the neutron star case with $V \sim c$. This spiral radius should be larger than the photosphere; otherwise, the wind eventually shields the line of sight as shown in Figure 1. This condition is marginally satisfied for the massive star case as the photospheric radius is $r_{\rm ph} \sim (10^{13}$–$10^{14})$ cm in Equations (5) and (8), while it is satisfied for the neutron star case. We can also predict a lack of sources with $P_{\rm orb} \lesssim 10$ days for the massive star case and $P_{\rm orb} \lesssim 0.1$ days (with some dependence on Γ and σ) for the neutron star case.

[6] If the inclination is close to face-on, the opening angle should be larger than Equation (13).

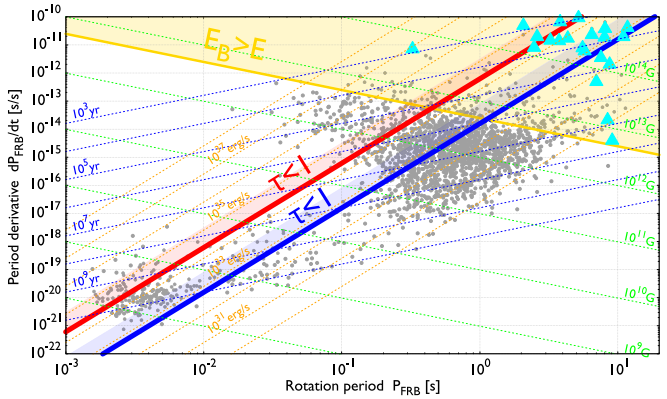

Figure 2. FRB pulsar in P–$\dot{P}$ diagram, satisfying the opacity constraint in Equation (20) for a massive star companion above the red bold line (where $\dot{P}_{\rm FRB} \propto \dot{M}_{-9}$ for different $\dot{M}$) and in Equation (21) for a neutron star companion above the blue bold line (where $\dot{P}_{\rm FRB} \propto L_{w,34}$ for different L_w). In the shaded region, the FRB pulsar is also combed by the wind from the companion. The energy constraint in Equation (23) is satisfied above the yellow solid line. The overlapped region contains magnetars (cyan triangles) and some pulsars (gray dots). Dotted lines show constant lifetime, magnetic field, and spin-down luminosity of pulsars.

3. Physical Properties of the FRB Pulsar

3.1. Opacity (Duty Cycle) Constraints

The comb size necessary for the duty cycle in Equation (15) is usually larger than that of the light cylinder of the FRB pulsar with a spin period $P_{\rm FRB} = 1\,{\rm s}\,P_{\rm FRB,0}$,

$$r_\ell \sim cP_{\rm FRB}/(2\pi) \sim 5 \times 10^9\,{\rm cm}\,P_{\rm FRB,0}. \quad (18)$$

Then the ram pressure balance between the winds from the companion and the FRB pulsar is expressed by

$$\frac{L_w}{4\pi a^2 V} \sim \frac{B_p^2}{8\pi}\left(\frac{R}{r_\ell}\right)^6\left(\frac{r_\ell}{r_0}\right)^2, \quad (19)$$

where $R \sim 10$ km is the neutron star radius, $L_w \sim \dot{M}V^2$ for the massive star case, and $V \approx c$ for the neutron star case. For the massive star case, the opacity condition in Equation (15) gives

$$B_p \gtrsim 3 \times 10^{13}\,{\rm G}\,P_{\rm FRB,0}^2 \dot{M}_{-9}^{1/2} V_{3.3}^{1/2}, \quad (20)$$

where the equality holds if the comb also stimulates an FRB in Equation (16). For the neutron star case, Equation (15) gives

$$B_p \gtrsim 4 \times 10^{12}\,{\rm G}\,P_{\rm FRB,0}^2 L_{w,34}^{1/2}, \quad (21)$$

where the equality holds if Equation (16) is also true. These conditions are presented in Figure 2.

3.2. Energetics Constraints

The total energy of FRBs during the whole lifetime $t_{\rm life} = 10^4$ yr $t_{\rm life,4}$ is

$$E = \dot{N}t_{\rm life}L\Delta t(\Delta\Omega/4\pi) \sim 4 \times 10^{42}\,{\rm erg}\,\dot{N}_{25}t_{\rm life,4}(L\Delta t)_{38}\Delta\Omega_{0.6\pi}, \quad (22)$$

where the observed burst rate is $\dot{N} \sim 25\ {\rm yr}^{-1}\dot{N}_{25}$, the true energy of each burst is smaller by a factor of $\delta\Omega/4\pi$, and the total number of bursts is increased by a factor of $\Delta\Omega/\delta\Omega$ (Zhang 2020). We take $\Delta\Omega \sim 2\pi(1-\cos(\pi/4)) \sim 0.6\pi$ as a fiducial value as implied by the duty cycle in Equation (13). This energy can be supplied by the magnetic energy $E_B > E$ if

$$B_p \gtrsim 5 \times 10^{12}\,{\rm G}\,\dot{N}_{25}^{1/2} t_{\rm life,4}^{1/2}(L\Delta t)_{38}^{1/2}\Delta\Omega_{0.6\pi}^{1/2}. \quad (23)$$

This is marked as the yellow shaded region in Figure 2.[7]

Combining Equations (20), (21), and (23), we find the FRB pulsar parameters in the range that includes magnetars and young high-B pulsars with $B_p \sim 10^{13}$–10^{15} G and $P_{\rm FRB} \sim$ 1–10 s for a lifetime $t_{\rm life} \sim 10^4$ yr (Figure 2). With these parameters, the FRB pulsar has enough energy and enough luminosity for pertaining a funnel in the wind from the companion while it is still combed by the wind to trigger FRBs.

Notice that Galactic binary neutron star systems do not satisfy the energy constraint in Equation (23), because their ages are much older, i.e., $t_{\rm life} \gg 10^4$ yr (e.g., Tauris et al. 2017). Gamma-ray binary systems such as PSR B1259-63 (Aharonian et al. 2005) and PSR J2032+4127 (Lyne et al. 2015) also do not satisfy the energy constraint. Only a relatively new born pulsar could have crust or magnetic configurations that can frequently trigger FRBs via crust cracking or magnetic reconnection. These intrinsic triggering factors could also explain why weaker Galactic analogs are not observed. The pulsar B of the double pulsar system J0737-3039 has $P_{\rm FRB} \sim 2.7735$ s and $B_p = 4.9 \times 10^{11}$ G. It also does not satisfy the opacity constraint in Equation (21). The Galactic high-mass X-ray binaries do not satisfy the opacity constraint because the neutron stars are accreting matter. Although many Galactic neutron stars satisfy both the opacity and energy constraints, they are not in binaries. In any case, we do not exclude the possibility that Galactic binary neutron star systems may emit FRB-like signals with much lower luminosities at a much lower rate. Detections or nondetections of such signals in long-term monitoring of these systems may lend support or pose constraints on the scenario proposed in this Letter.

3.3. FRB Emission

From the opacity constraint, the interaction radius in Equation (15) is larger than the light cylinder in Equation (18). The magnetic field at the interaction radius is weaker than that of the inner magnetosphere near the neutron star surface where the most energy E_B is stored to produce an FRB. Then binary interactions cannot change the inner magnetic structure to trigger an FRB unless a much tighter binary system is invoked. In Earth's magnetosphere, for example, magnetic reconnection takes place in the dayside magnetopause and the near-Earth plasma sheet. No reconnection happens near Earth's surface.

On the other hand, binary interactions may change the current structure (electron density) in the inner magnetosphere, which may be related to the coherent condition for FRB emission. In intermittent pulsars (Kramer et al. 2006) and mode-switching pulsars (Lyne et al. 2010), the change of the spin-down rate (possibly related to the change of the magnetospheric structure) is connected with the change of the radio emission condition.

Based on the energy budget argument, the FRB energy should be dissipated from the inner magnetosphere of the FRB pulsar itself, likely due to crust cracking or magnetic

[7] Notice that the spin-down luminosity of a pulsar is usually much smaller than the isotropic FRB luminosity (e.g., Muñoz et al. 2020), so that the magnetic energy is most likely the prime mover of FRBs unless the FRB is very narrowly collimated (Katz 2018).

reconnection. This intrinsic trigger would be similar to that of ordinary magnetars or young, high-magnetic-field pulsars. However, we speculate that binary interaction may provide the condition to facilitate the FRB coherent radiation mechanism, so that only a small fraction of the intrinsic trigger events can lead to FRBs (see Section 4.2 for more detailed arguments). The interface of the interaction region and the light cylinder of the FRB pulsar makes a connection between the external wind and inner magnetosphere (see Figure 1), powering an aurora (Perreault & Akasofu 1978; Ebihara & Tanaka 2020) or lightening (Scott et al. 2014) similar to that in Earth's magnetosphere. Possibly the massive star companion provides substantial seed photons for creating high-energy particles. The sudden release of energy in the inner magnetosphere launches a strong particle outflow. When this outflow interacts with the aurora plasma, two-stream instability may drive particle bunches that meet the coherent condition for FRBs (Kashiyama et al. 2013; Kumar et al. 2017; Yang & Zhang 2018). Alternatively, coherent radiation may be generated by the conversion from reconnection-driven fast magnetosonic waves to electromagnetic waves (Philippov et al. 2019; Lyubarsky 2020). The aurora particles might change the physical parameters such as the conversion radius and Lorentz factor, and hence the coherent condition. These mechanisms can reproduce the FRB properties such as polarization and downward-drifting subpulses (Wang et al. 2019).

4. Other Constraints

4.1. DM, RM, and Persistent Emission

For FRB 180916.J0158+6, the change of dispersion measure (DM) is constrained as $\Delta\mathrm{DM} < 0.1$ pc cm^{-3} (The CHIME/FRB Collaboration et al. 2020). This is easily satisfied for the neutron star companion case. For the massive star companion case, the contribution to ΔDM only comes from the radius beyond the photosphere. Considering the difference in the path length during the 4 day active phase, we find that the DM variation is limited by

$$\Delta\mathrm{DM} \lesssim n_w(r_{\rm ph}) r_{\rm ph}[1-\cos(\pi/4)] \sim 0.05\ \mathrm{pc\ cm^{-3}}\, M_{-9} V_{3.3}^{-1} r_{\rm ph,14}^{-1}, \quad (24)$$

which is consistent with the observation. More precise observations could detect the DM variation. Note that at the photosphere, the electric field of the FRB radiation is too weak to accelerate electrons to relativistic energies on the timescale of $(2\pi\nu)^{-1}$ to reduce the DM (Lu & Phinney 2019; Yang & Zhang 2020). The outflow associated with FRBs could also bring additional ΔDM (Yamasaki et al. 2019).

We expect an even larger mass-loss rate for a more massive star and, hence, a larger ΔDM. Thus, a main-sequence B star companion is preferred for the periodic FRB 180916.J0158+65. About 20 CHIME bursts do not show a large ΔDM, possibly except for source 5 in Fonseca et al. (2020). Since more massive stars are less abundant, this observation is consistent with our scenario, even though more samples are needed to verify the massive star companion case.

The rotation measure (RM) of the source is measured as RM $\sim -114.6 \pm 0.6$ rad m^{-2} (CHIME/FRB Collaboration et al. 2019). For the neutron star companion case, the expected RM is small. For the massive star companion case, there is no evidence of magnetic field for Be stars, and the dipole field component of 50% of the stars is probably weaker than 50 G (Wade et al. 2014). At the photosphere, this corresponds to $\lesssim 50\ \mathrm{G}\ (3\times10^{11}\ \mathrm{cm}/r_{\rm ph})^2 \sim 5\times10^{-4}$ G. The expected absolute value of RM is $\sim q^3(2\pi m^2c^4)^{-1}\int_{r_{\rm ph}} n_w B_\parallel dr \lesssim 20$ rad m^{-2}, less than the observations. The nondetection of RM variation implies that the RM comes from a further distance such as the persistent emission region (Yang et al. 2020).

The persistent radio counterpart is constrained to have a luminosity $\nu L_\nu < 1.3\times10^{36}$ erg s^{-1} at 1.7 GHz by the continuum EVN data and $\nu L_\nu < 7.6\times10^{35}$ erg s^{-1} at 1.6 GHz by the VLA data (Marcote et al. 2020). In our model the wind luminosities are less than these constraints. In the massive star case, the companion mainly shines in the optical band, also consistent with the observations.

4.2. Event Rate Density

Given the burst fluxes $\sim$1 Jy and the distance to the periodic FRB $\sim$149 Mpc (The CHIME/FRB Collaboration et al. 2020), a typical luminosity of each burst is $L \sim 10^{40}$ erg s^{-1}. At this luminosity, the event rate density from all the observed FRBs is about

$$\mathcal{R}_{\rm FRB}(>L) \lesssim \int_L \phi(L)dL \sim 10^6\ \mathrm{Gpc^{-3}\ yr^{-1}} L_{40}^{-0.8} \quad (25)$$

by extrapolating and integrating the luminosity function derived from FRBs above 10^{42} erg s^{-1} (Luo et al. 2020): $\phi(L)dL = \phi^*(L/L^*)^\alpha \exp(-L/L^*)dL/L^*$, where $\alpha = -1.8$, $\phi^* \sim 339$ Gpc^{-3} yr^{-1} and $L^* \sim 2.9\times10^{44}$ erg s^{-1}. Here the "$\lesssim$" sign in Equation (25) denotes the possibility of a luminosity function cutoff below 10^{42} erg s^{-1}. We note that if this is the case, the argument below is even tighter, so that the current estimate is rather conservative.

If the majority of observed FRBs are dominantly produced by similar sources discussed in this Letter, the true volumetric birth rate of such sources is

$$\mathscr{R} \sim \frac{\mathcal{R}_{\rm FRB}}{\dot{N} t_{\rm life}} \frac{4\pi}{\Delta\Omega} \lesssim 30\ \mathrm{Gpc^{-3}\ yr^{-1}}\, \dot{N}_{25}^{-1} t_{\rm life,4}^{-1} \Delta\Omega_{0.6\pi}^{-1}. \quad (26)$$

This is much smaller than the supernova rate density $\sim10^5$ Gpc^{-3} yr^{-1} and the magnetar birth rate density $\sim10^4$ Gpc^{-3} yr^{-1} (Kaspi & Beloborodov 2017) for a reasonable lifetime $t_{\rm life} \gg 1$ yr. The expected number of FRB sources is only $\lesssim 0.03\dot{N}_{25}^{-1}\Delta\Omega_{0.6\pi}^{-1}$ in our Galaxy. This suggests that a special condition is necessary to limit the amount of sources to produce FRBs and binary interaction is an attractive solution. Thus, our model is not like a single magnetar model. Binary interaction is an important ingredient of the model.

For the massive star companion case, the reduction factors from the supernova rate density include the fraction of pulsars that satisfies the FRB condition (may be comparable to the magnetar fraction) by $\sim$0.1 (Kaspi & Beloborodov 2017), the fraction of the right binary separation by $\sim$0.1 (Moe & Di Stefano 2017), the survival fraction of the kick at the first supernova by $\sim$0.1 (Postnov & Yungelson 2014; Tauris et al. 2017), the mass ratio and so on by $\sim$0.3 (Moe & Di Stefano 2017). Thus, it is natural to have a small birth rate similar to Equation (26).

For the neutron star companion case, the birth rate of binary neutron stars with a separation of $a \sim 10^{12}$ cm is estimated as $\sim10^2$ Gpc^{-3} yr^{-1} by the population synthesis (Belczynski et al. 2002), which is smaller by a factor of $\sim$10 than the merger rate

derived from gravitational-wave observations (Abbott et al. 2017, 2020). This is also consistent with the number of Galactic binary neutron star systems (Tauris et al. 2017). By multiplying the magnetar fraction ∼0.1, it also gives a small birth rate similar to Equation (26).

5. Summary and Discussions

We have shown that if the periodicity of FRB 180916.J0158+65 is due to the binary period, the interaction between a young, strongly magnetized neutron star (the FRB pulsar) and a companion with a strong wind can give the right conditions to interpret the observations. The wind from the companion makes the system optically thick to FRB photons due to induced Compton or Raman scatterings. The FRB pulsar should make a clear funnel by blowing a wind, which is preserved by a cosmic comb of the FRB pulsar magnetic field. The production of FRBs requires that the FRB pulsar be young and highly magnetized. Since supernova explosions provide too high a birth rate density that may overproduce repeating FRBs, a special condition may be required to facilitate FRB production. We suggest that interactions in binary systems may be essential to generate FRBs besides the intrinsic conditions (strong magnetic fields and young age) imposed on the FRB pulsars.

We predict a lack of FRBs with $P_{\rm orb} \lesssim 10$ days for a massive star companion and $P_{\rm orb} \lesssim 0.1$ days (with some dependence on Γ and σ) for a neutron star companion, because the funnel is spiraled by the orbital motion within the photosphere in those cases. We also suggest that a DM variation is close to the detection limit for the massive star case, requiring more samples with the precision of measurements.

The periodic FRB 180916.J0158+65 is apparently different from the first repeater FRB 121102, which emits bright FRBs and is accompanied by a bright persistent source $\sim 10^{39}$ erg s^{-1} and high $|{\rm RM}| \sim 10^5$ rad m^{-2} (Spitler et al. 2016; Chatterjee et al. 2017; Marcote et al. 2017; Tendulkar et al. 2017). That source may imply a different type of companion such as a supermassive black hole (Zhang 2018).[8]

There might exist genuinely non-repeating FRBs that comprise a small fraction of the total FRB population, but with distinct emission properties (e.g., non-repeating FRB pulses appear to be narrower than repeating ones; CHIME/FRB Collaboration et al. 2019; Fonseca et al. 2020). These bursts may have catastrophic origins such as neutron star mergers (Totani 2013), white dwarf mergers (Kashiyama et al. 2013), and so on.

The authors would like to thank the anonymous referee for useful comments, and H. Gao, W. Ishizaki, K. Kashiyama, S. Kisaka, P. Kumar, K. Kyutoku, K. Murase, N. Seto, S. Shibata, Y. Suwa, S. Tanaka, and C. Thompson for useful discussions. This research made use of the ATNF pulsar catalog (https://www.atnf.csiro.au/research/pulsar/psrcat/; Manchester et al. 2005) and McGill Online Magnetar Catalog (http://www.physics.mcgill.ca/~pulsar/magnetar/main.html; Olausen & Kaspi 2014). This work is partly supported by JSPS KAKENHI Nos. 18H01215, 17H06357, 17H06362, 17H06131, 26287051 (K.I.). Discussions during the YITP workshop YITP-T-19-04 and YKIS2019 were also useful to complete this work. B.Z. acknowledges UNLV for granting a sabbatical leave and YITP for hospitality and support.

[8] Possible periodic activity was also reported for FRB 121102 (Rajwade et al. 2020) after the submission of this Letter.

ORCID iDs

Kunihito Ioka https://orcid.org/0000-0002-3517-1956
Bing Zhang https://orcid.org/0000-0002-9725-2524

References

Abbott, B. P., Abbott, R., Abbott, T. D., et al. 2017, PhRvL, 119, 161101
Abbott, B. P., Abbott, R., Abbott, T. D., et al. 2020, arXiv:2001.01761
Aharonian, F., Akhperjanian, A. G., Aye, K. M., et al. 2005, A&A, 442, 1
Belczynski, K., Kalogera, V., & Bulik, T. 2002, ApJ, 572, 407
Bucciantini, N. 2002, A&A, 387, 1066
Chatterjee, S., Law, C. J., Wharton, R. S., et al. 2017, Natur, 541, 58
CHIME/FRB Collaboration, Andersen, B. C., Bandura, K., et al. 2019, ApJL, 885, L24
Cordes, J. M., & Chatterjee, S. 2019, ARA&A, 57, 417
Ebihara, Y., & Tanaka, T. 2020, RvMPP, 4, 2
Fonseca, E., Andersen, B. C., Bhardwaj, M., et al. 2020, ApJL, 891, L6
Inoue, S. 2004, MNRAS, 348, 999
Ioka, K. 2003, ApJL, 598, L79
Kashiyama, K., Ioka, K., & Mészáros, P. 2013, ApJL, 776, L39
Kashiyama, K., & Murase, K. 2017, ApJL, 839, L3
Kaspi, V. M., & Beloborodov, A. M. 2017, ARA&A, 55, 261
Katz, J. I. 2016, ApJ, 826, 226
Katz, J. I. 2018, PrPNP, 103, 1
Katz, J. I. 2020, MNRAS, 494, 64
Kippenhahn, R., & Weigert, A. 1990, Stellar Structure and Evolution (Berlin: Springer)
Kramer, M., Lyne, A. G., O'Brien, J. T., Jordan, C. A., & Lorimer, D. R. 2006, Sci, 312, 549
Kumar, P., Lu, W., & Bhattacharya, M. 2017, MNRAS, 468, 2726
Levin, Y., Beloborodov, A. M., & Bransgrove, A. 2020, arXiv:2002.04595
Lorimer, D. R., Bailes, M., McLaughlin, M. A., Narkevic, D. J., & Crawford, F. 2007, Sci, 318, 777
Lu, W., & Phinney, E. S. 2019, arXiv:1912.12241
Luo, R., Men, Y., Lee, K., et al. 2020, MNRAS, in press
Lyne, A., Hobbs, G., Kramer, M., Stairs, I., & Stappers, B. 2010, Sci, 329, 408
Lyne, A. G., Stappers, B. W., Keith, M. J., et al. 2015, MNRAS, 451, 581
Lyubarsky, Y. 2008, ApJ, 682, 1443
Lyubarsky, Y. 2020, arXiv:2001.02007
Lyutikov, M., Barkov, M., & Giannios, D. 2020, arXiv:2002.01920
Manchester, R. N., Hobbs, G. B., Teoh, A., & Hobbs, M. 2005, AJ, 129, 1993
Marcote, B., Nimmo, K., Hessels, J. W. T., et al. 2020, Natur, 577, 190
Marcote, B., Paragi, Z., Hessels, J. W. T., et al. 2017, ApJL, 834, L8
Metzger, B. D., Berger, E., & Margalit, B. 2017, ApJ, 841, 14
Moe, M., & Di Stefano, R. 2017, ApJS, 230, 15
Muñoz, J. B., Ravi, V., & Loeb, A. 2020, ApJ, 890, 162
Murase, K., Kashiyama, K., & Mészáros, P. 2016, MNRAS, 461, 1498
Nieuwenhuijzen, H., & de Jager, C. 1988, A&A, 203, 355
Olausen, S. A., & Kaspi, V. M. 2014, ApJS, 212, 6
Perreault, P., & Akasofu, S. I. 1978, GeoJ, 54, 547
Petroff, E., Hessels, J. W. T., & Lorimer, D. R. 2019, A&ARv, 27, 4
Philippov, A., Uzdensky, D. A., Spitkovsky, A., & Cerutti, B. 2019, ApJL, 876, L6
Popov, S. B., & Postnov, K. A. 2013, arXiv:1307.4924
Postnov, K. A., & Yungelson, L. R. 2014, LRR, 17, 3
Puls, J., Vink, J. S., & Najarro, F. 2008, A&ARv, 16, 209
Rajwade, K. M., Mickaliger, M. B., Stappers, B. W., et al. 2020, arXiv:2003.03596
Scott, C. J., Harrison, R. G., Owens, M. J., Lockwood, M., & Barnard, L. 2014, ERL, 9, 055004
Smith, N. 2014, ARA&A, 52, 487
Spitler, L. G., Scholz, P., Hessels, J. W. T., et al. 2016, Natur, 531, 202
Tauris, T. M., Kramer, M., Freire, P. C. C., et al. 2017, ApJ, 846, 170
Tendulkar, S. P., Bassa, C. G., Cordes, J. M., et al. 2017, ApJL, 834, L7
The CHIME/FRB Collaboration, Amiri, M., Andersen, B. C., et al. 2020, arXiv:2001.10275
Thompson, C., Blandford, R. D., Evans, C. R., & Phinney, E. S. 1994, ApJ, 422, 304
Thornton, D., Stappers, B., Bailes, M., et al. 2013, Sci, 341, 53

Totani, T. 2013, PASJ, 65, L12
Vigelius, M., Melatos, A., Chatterjee, S., Gaensler, B. M., & Ghavamian, P. 2007, MNRAS, 374, 793
Wade, G. A., Petit, V., Grunhut, J., & Neiner, C. 2014, arXiv:1411.6165
Wang, W., Zhang, B., Chen, X., & Xu, R. 2019, ApJL, 876, L15
Wilkin, F. P. 1996, ApJL, 459, L31
Wilson, D. B., & Rees, M. J. 1978, MNRAS, 185, 297
Yamasaki, S., Kisaka, S., Terasawa, T., & Enoto, T. 2019, MNRAS, 483, 4175
Yang, H., & Zou, Y.-C. 2020, arXiv:2002.02553
Yang, Y.-P., Li, Q.-C., & Zhang, B. 2020, arXiv:2001.10761
Yang, Y.-P., & Zhang, B. 2018, ApJ, 868, 31
Yang, Y.-P., & Zhang, B. 2020, ApJL, 892, L10
Zanazzi, J. J., & Lai, D. 2020, ApJL, 892, L15
Zhang, B. 2017, ApJL, 836, L32
Zhang, B. 2018, ApJL, 854, L21
Zhang, B. 2020, ApJL, 890, L24